Supplementary Information

Placement of Tyrosine Residues as a Design Element for Tuning the Phase Transition of ELP-CLP conjugates: Experiments and Simulations

Phillip A. Taylor[1†], Haofu Huang[2†], Kristi L. Kiick[2*], Arthi Jayaraman[1,2*]

[1]Department of Chemical and Biomolecular Engineering, University of Delaware, Newark, DE 19716 USA
[2]Department of Materials Science and Engineering, University of Delaware, Newark, DE 19716 USA

*Corresponding Authors
Email: kiick@udel.edu, arthij@udel.edu

† Equal contributions.

Characterization results

All peptides were synthesized via solid-phase peptide synthesis methods (SPPS) as described in the main content. 4-azidobutanoic acid was introduced to the N-terminus of the CLP via amidation reaction. An alkyne group from propargyl glycine was attached to the C-terminus of the ELP domain via SPPS. The facile conjugation of ELP and CLP via CuAAC "click" reaction was conducted as described in the main content (Fig. 1). The molecular weight of CLP, ELPs & ELP-CLP conjugates was verified via electrospray ionization mass spectrometry (ESI-MS) (Figure S1-S13). After purification with reverse-phase HPLC, conjugates with purity greater than 95% were obtained (Figure S14 & S15). The two peaks that are apparent in the chromatograms below are a result of CLP triple helix formation which combines a fraction of the ELP-CLP monomer into trimers, while a fraction of the conjugates remain as monomers. This mixture of ELP-CLP trimers and monomers under the HPLC experimental conditions results in the two peaks in the HPLC chromatogram. Our ESI-MS data indicate that there are few to no impurities in any of the peptides synthesized.

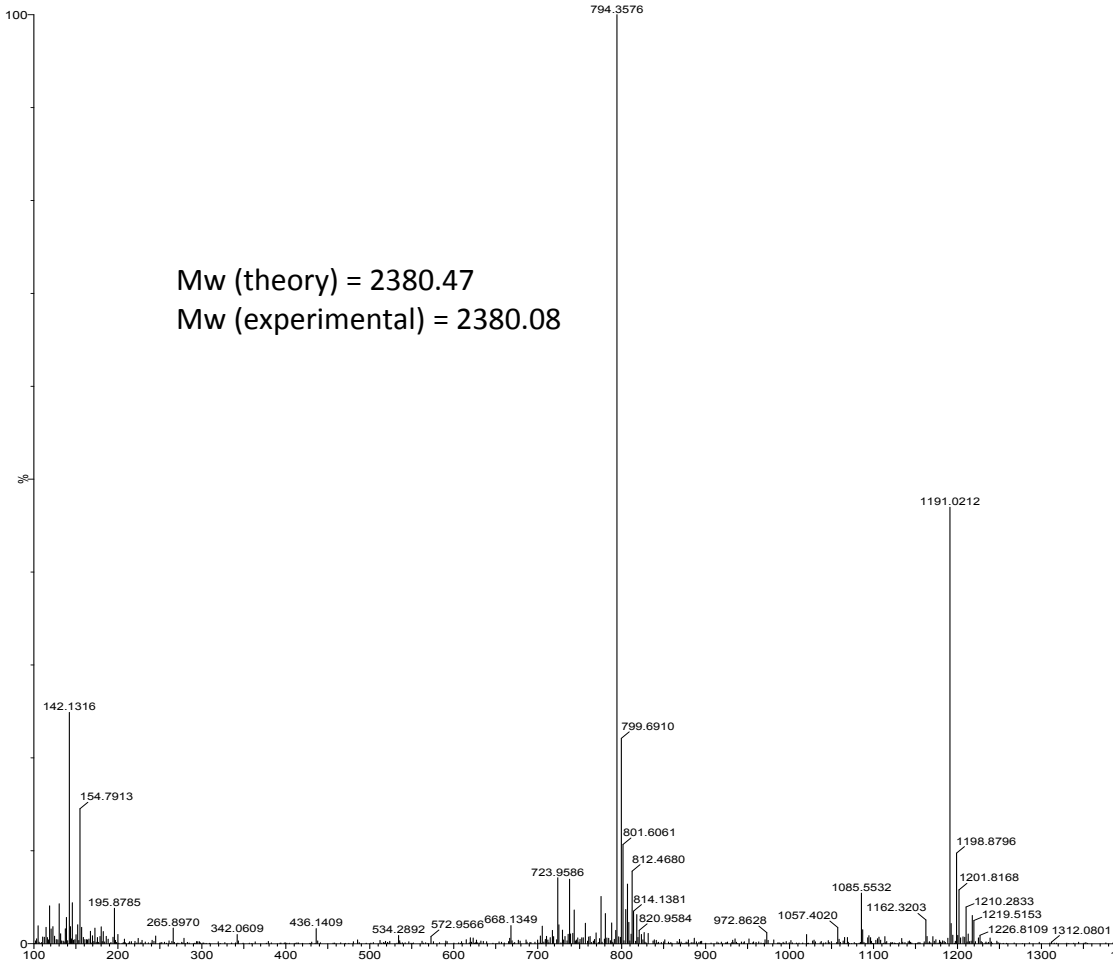

Figure S1 ESI-MS of purified G_8

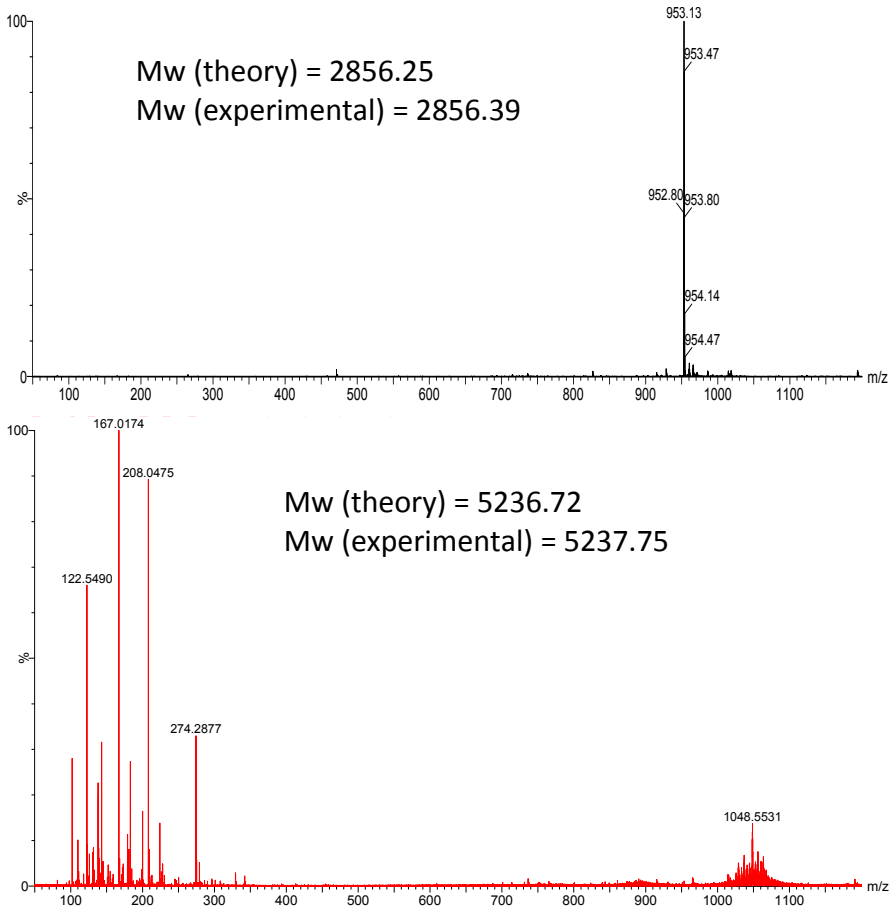

Figure S2 ESI-MS of purified: Top: F_6, Bottom: F_6-G_8

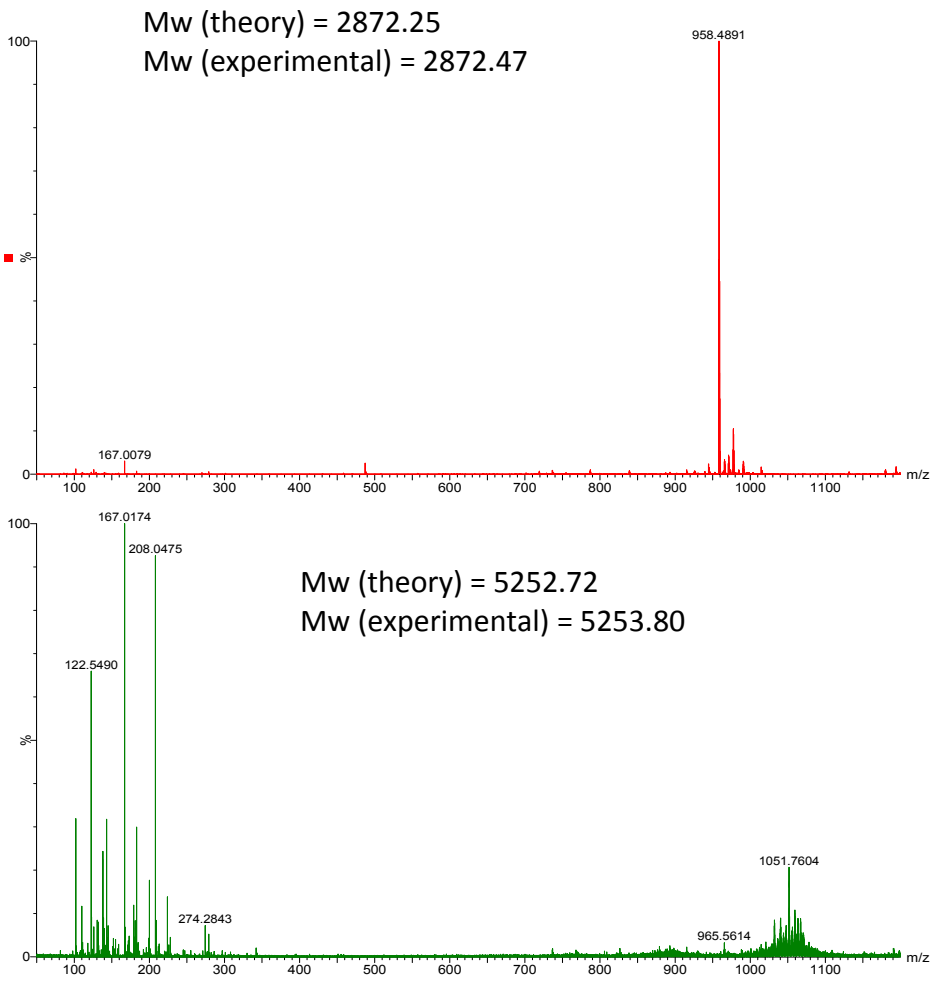

Figure S3 ESI-MS of purified: Top: F_5Y, Bottom: F_5Y-G_8

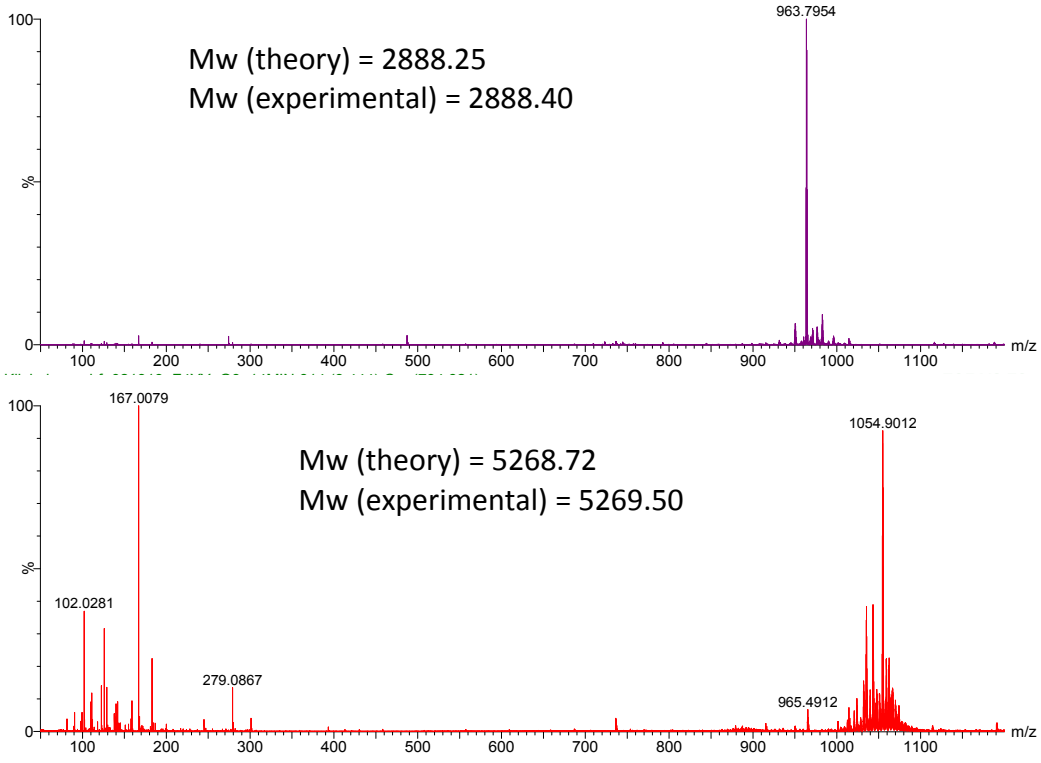

Figure S4 ESI-MS of purified: Top: F_4Y_2, Bottom: F_4Y_2-G_8

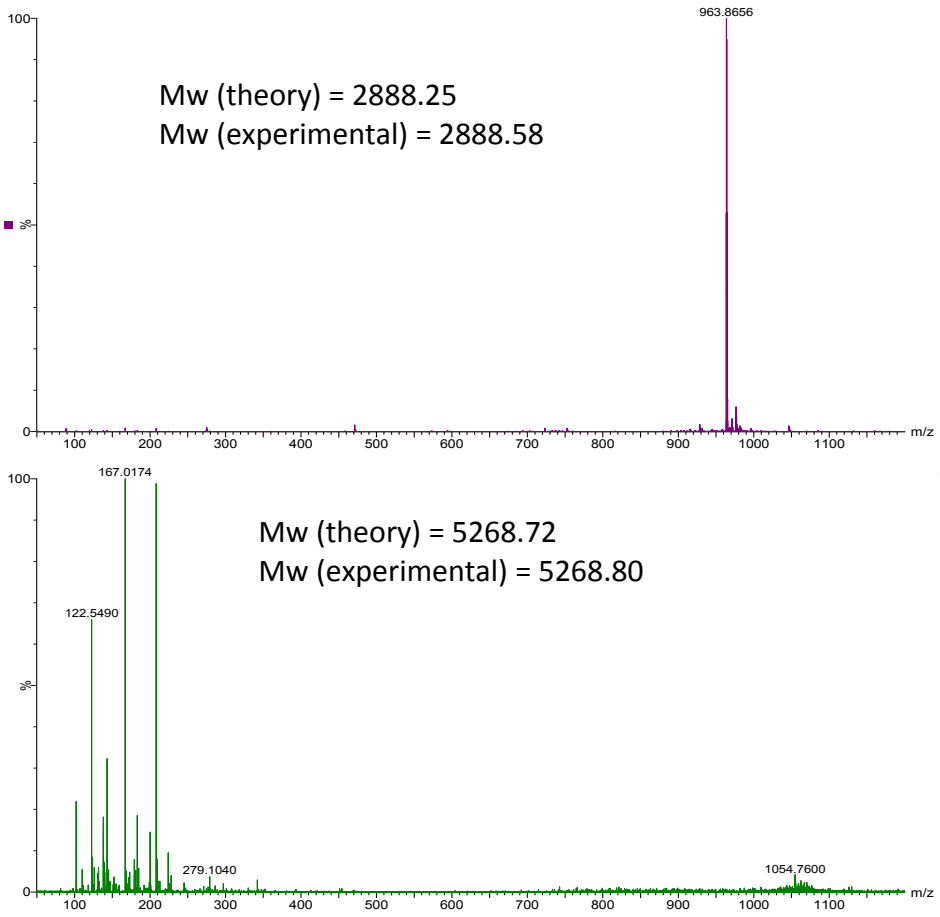

Figure S5 ESI-MS of purified: Top: Y_2F_4, Bottom: Y_2F_4-G_8

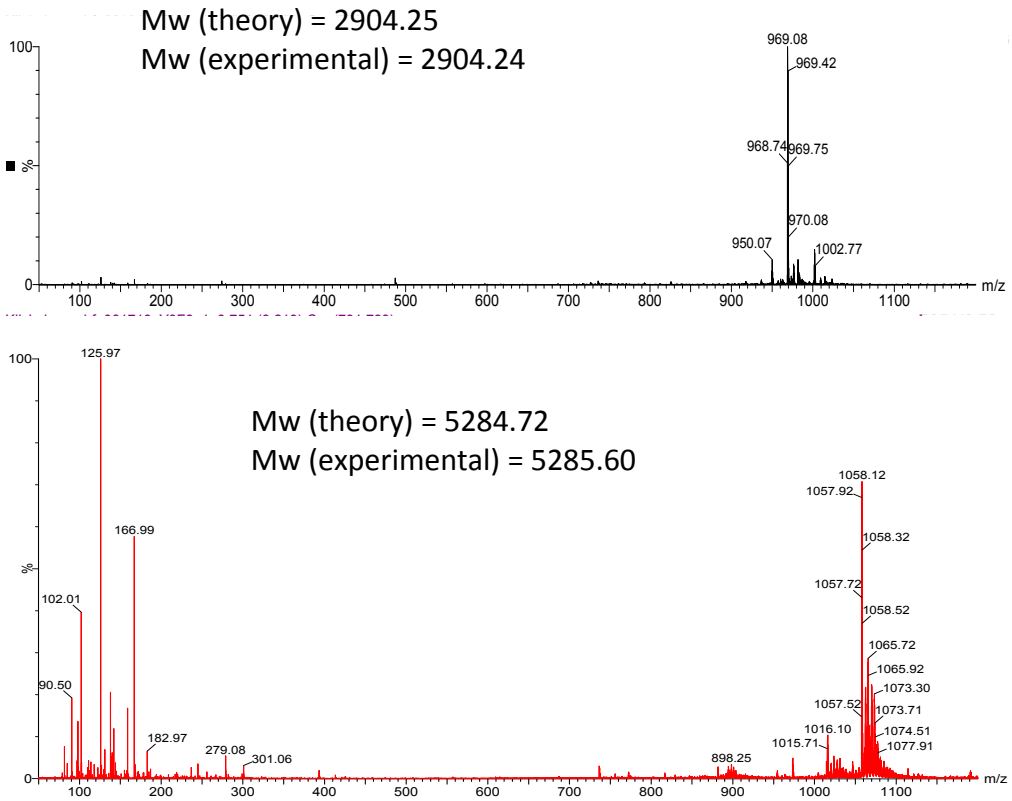

Figure S6 ESI-MS of purified: Top: F_3Y_3, Bottom: F_3Y_3-G_8

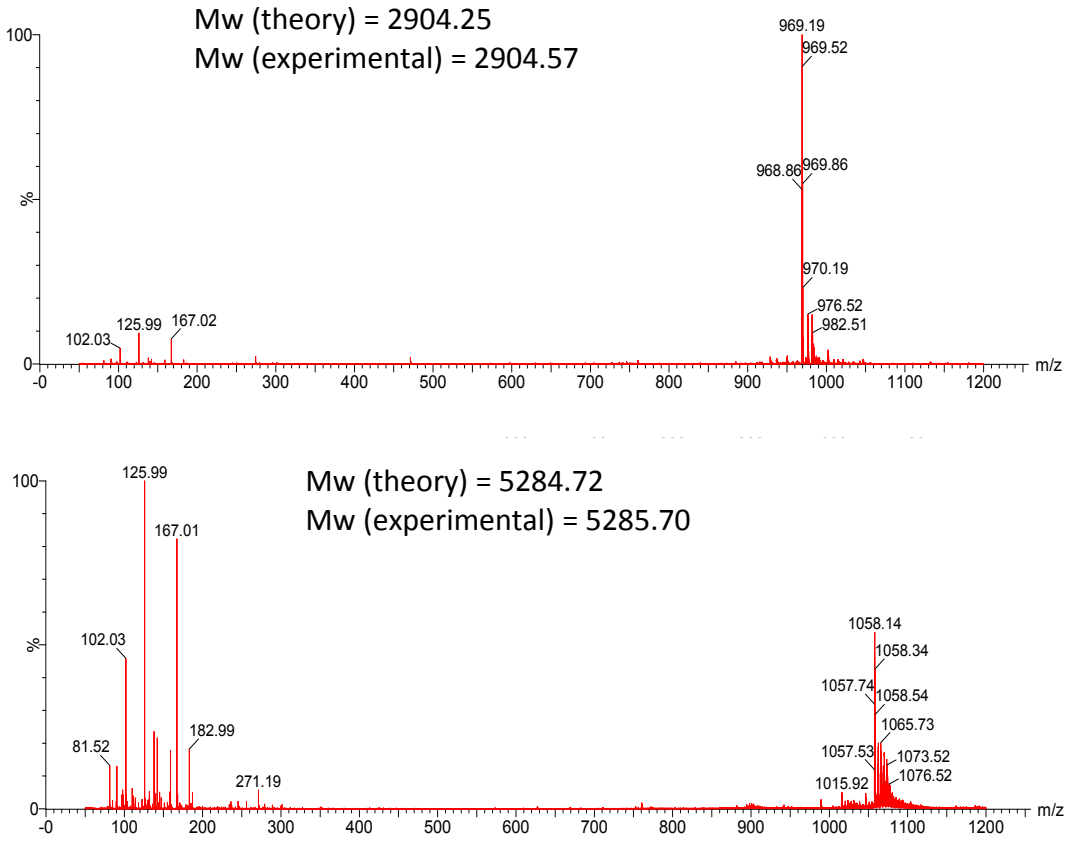

Figure S7 ESI-MS of purified: Top: Y_3F_3, Bottom: Y_3F_3-G_8

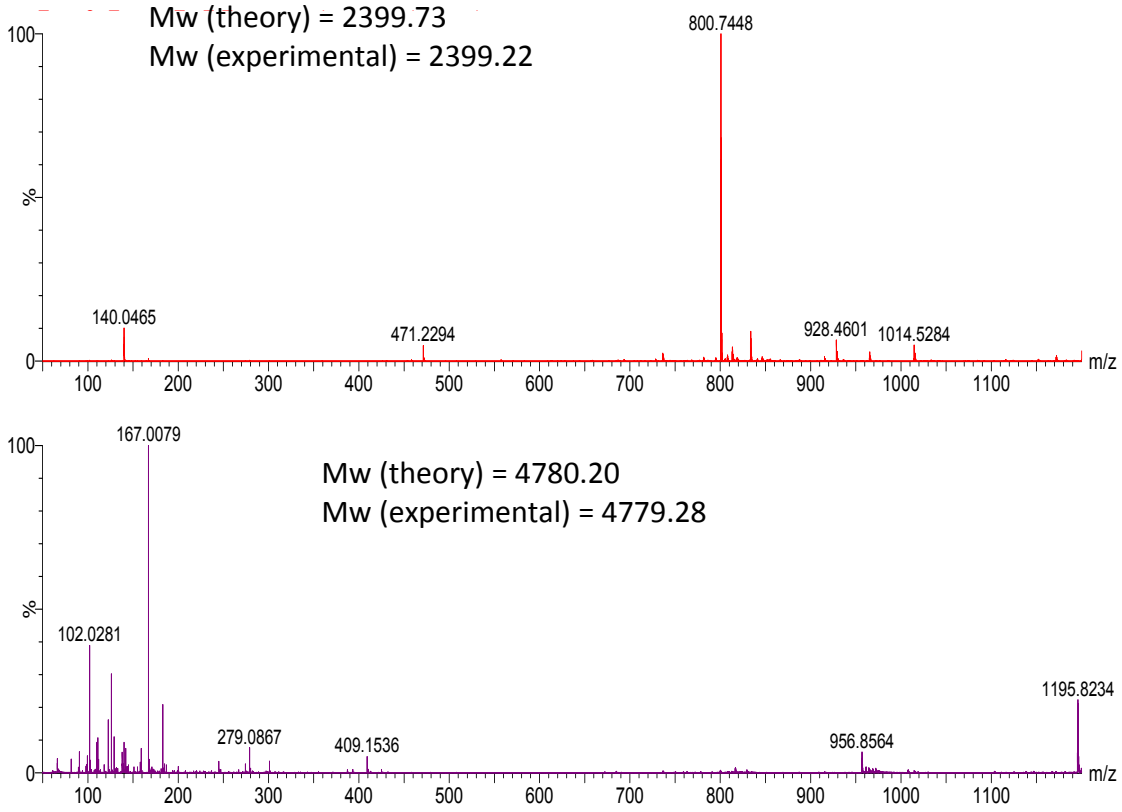

Figure S8 ESI-MS of purified: Top: F_5, Bottom: F_5-G_8

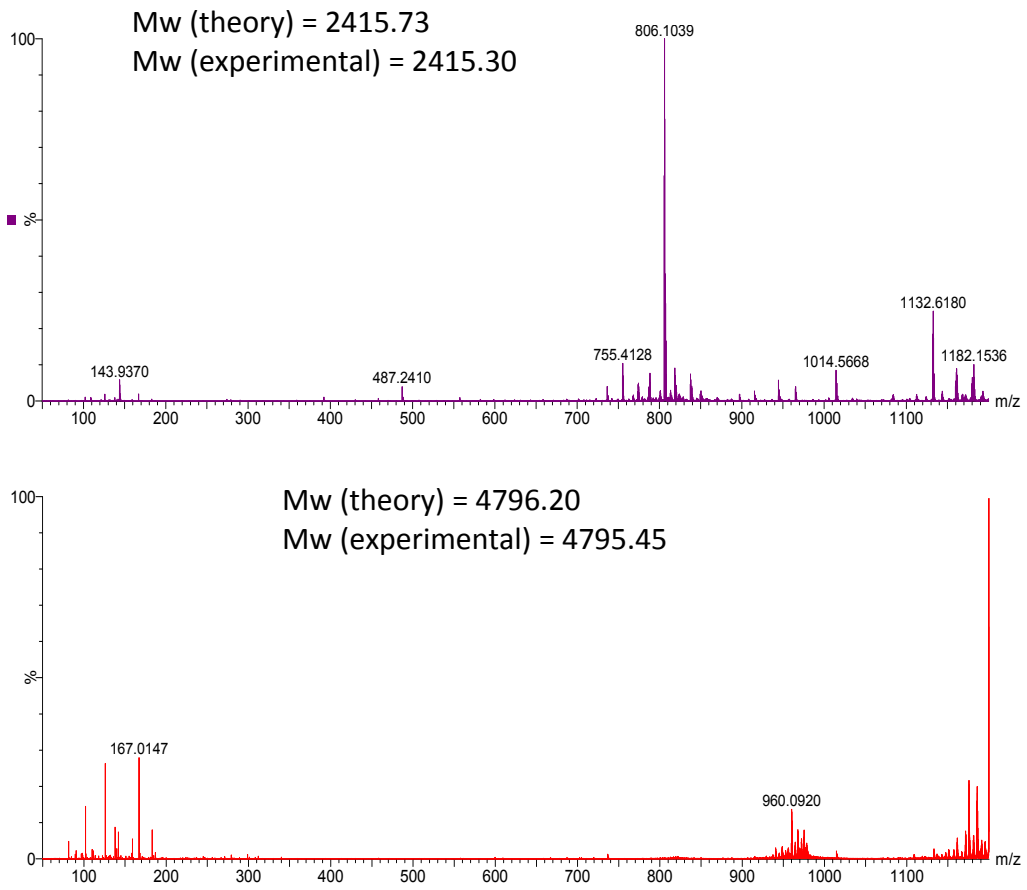

Figure S9 ESI-MS of purified: Top: F_4Y, Bottom: F_4Y-G_8

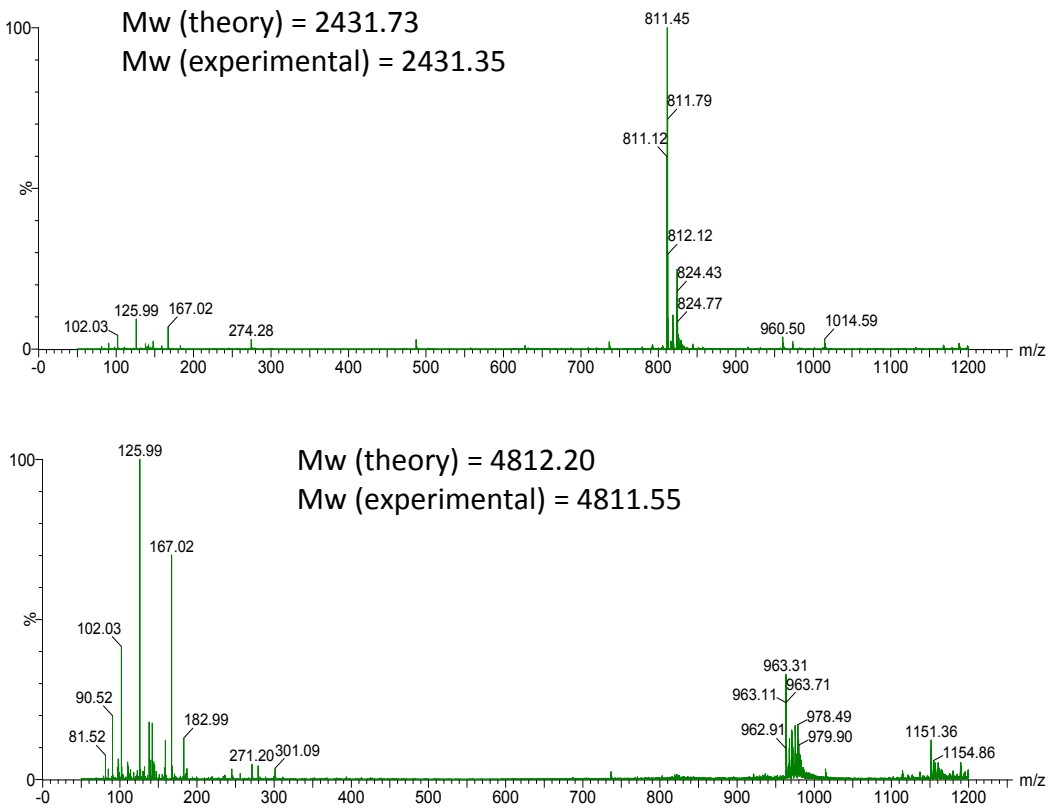

Figure S10 ESI-MS of purified: Top: F_3Y_2, Bottom: F_3Y_2-G_8

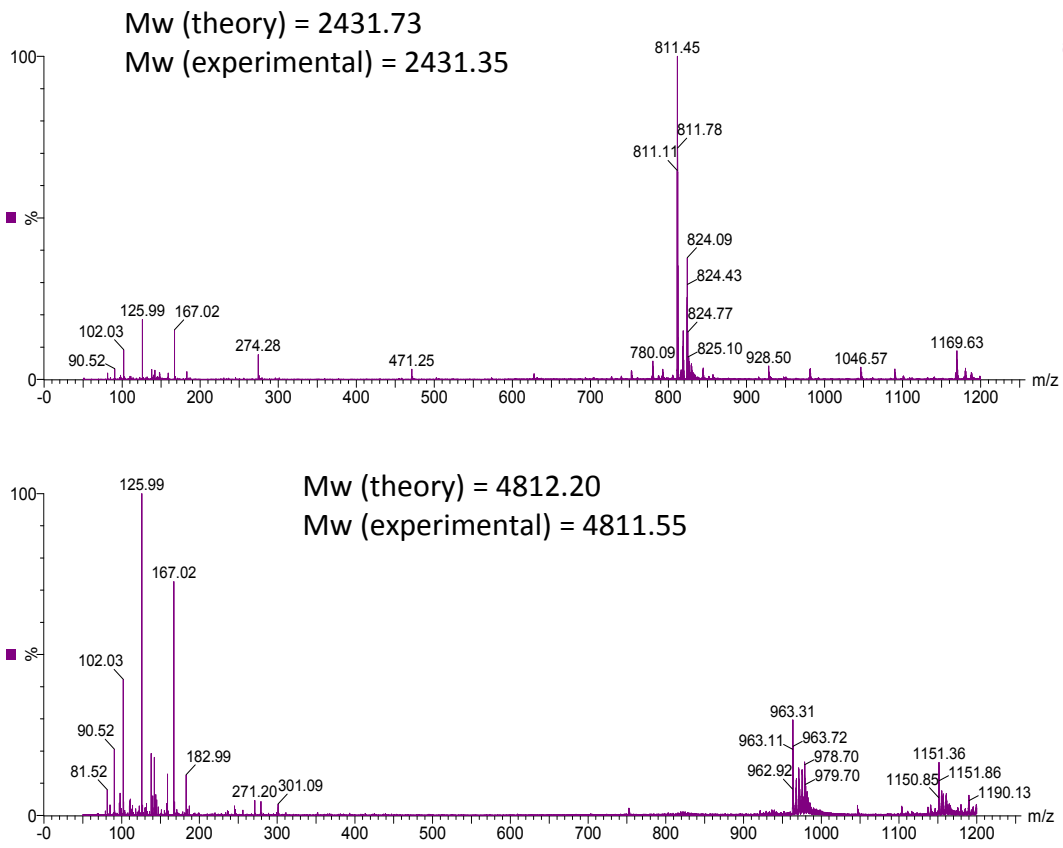

Figure S11 ESI-MS of purified: Top: Y_2F_3, Bottom: Y_2F_3-G_8

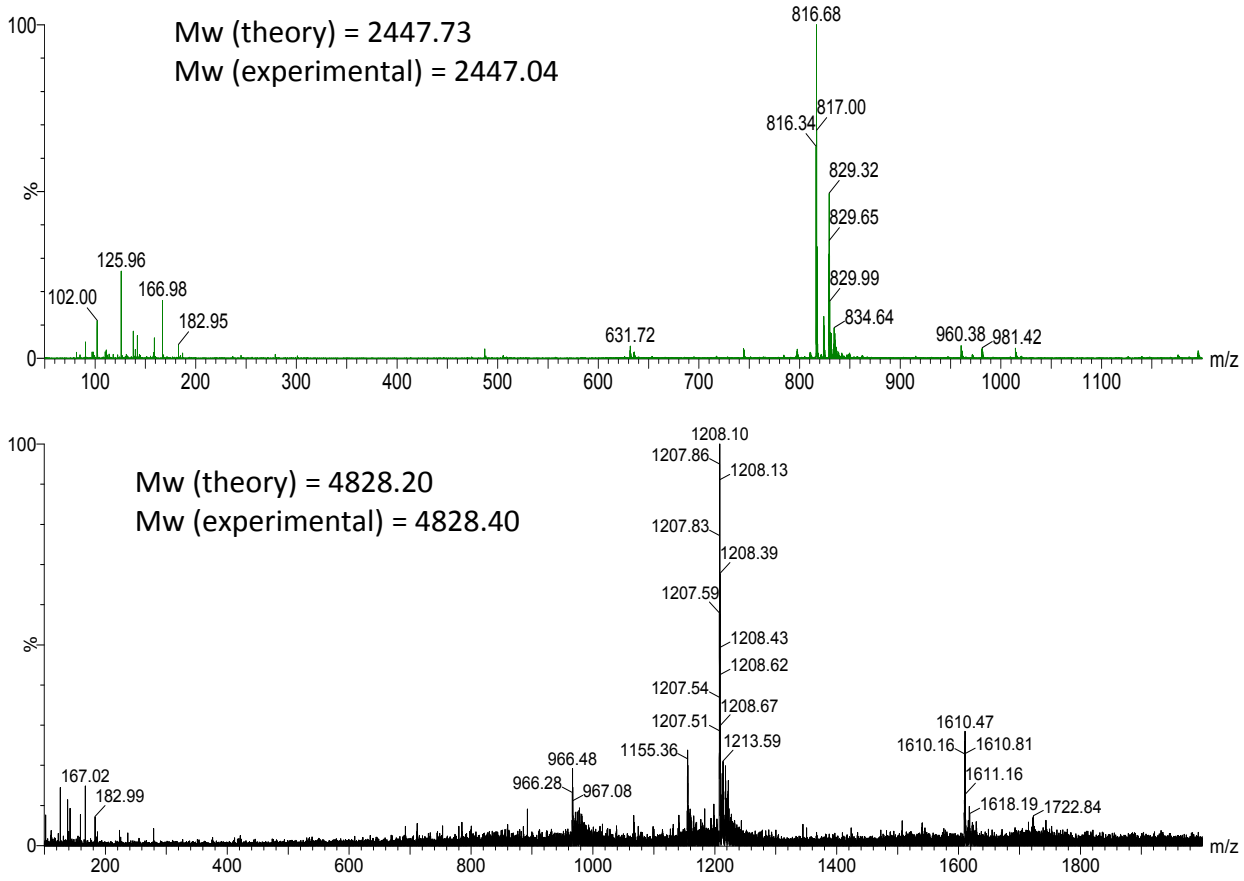

Figure S12 ESI-MS of purified: Top: F_2Y_3, Bottom: F_2Y_3-G_8

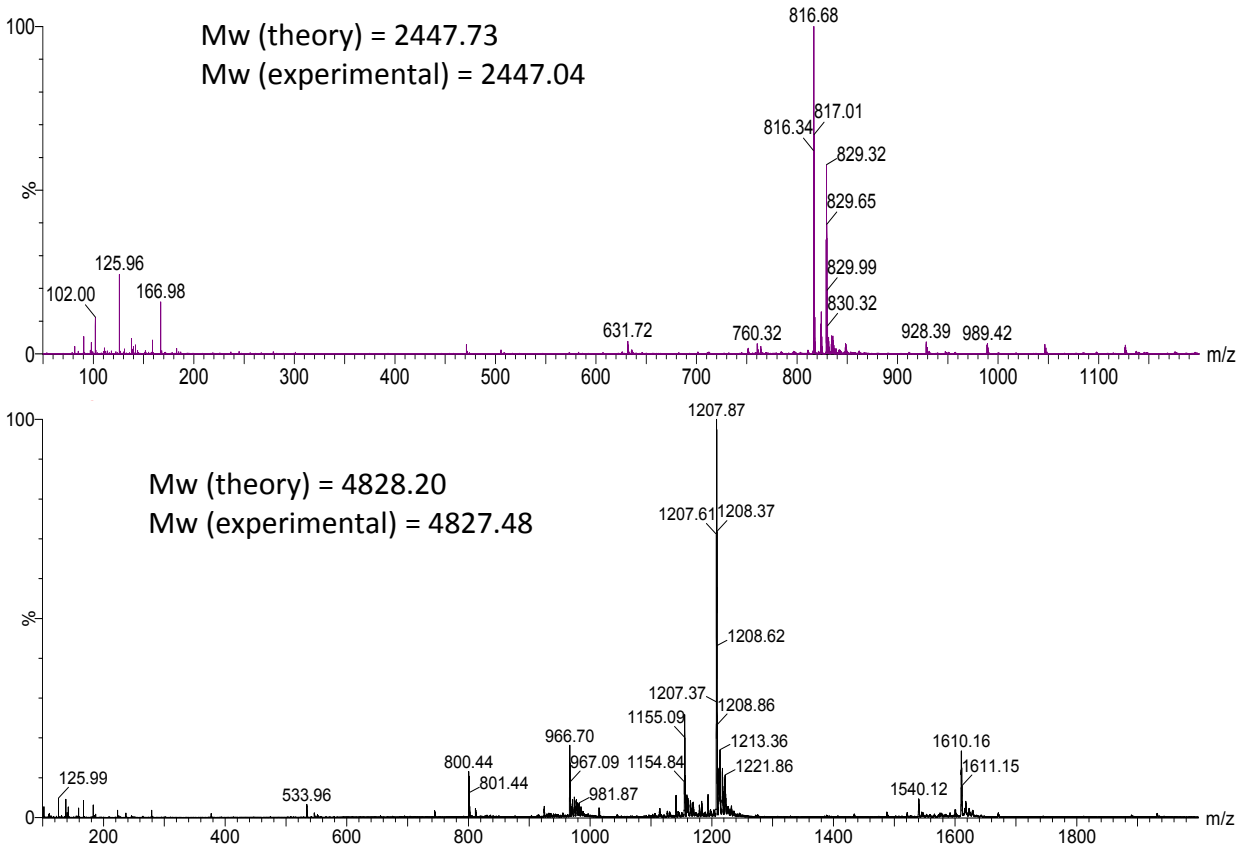

Figure S13 ESI-MS of purified: Top: Y_3F_2, Bottom: Y_3F_2-G_8

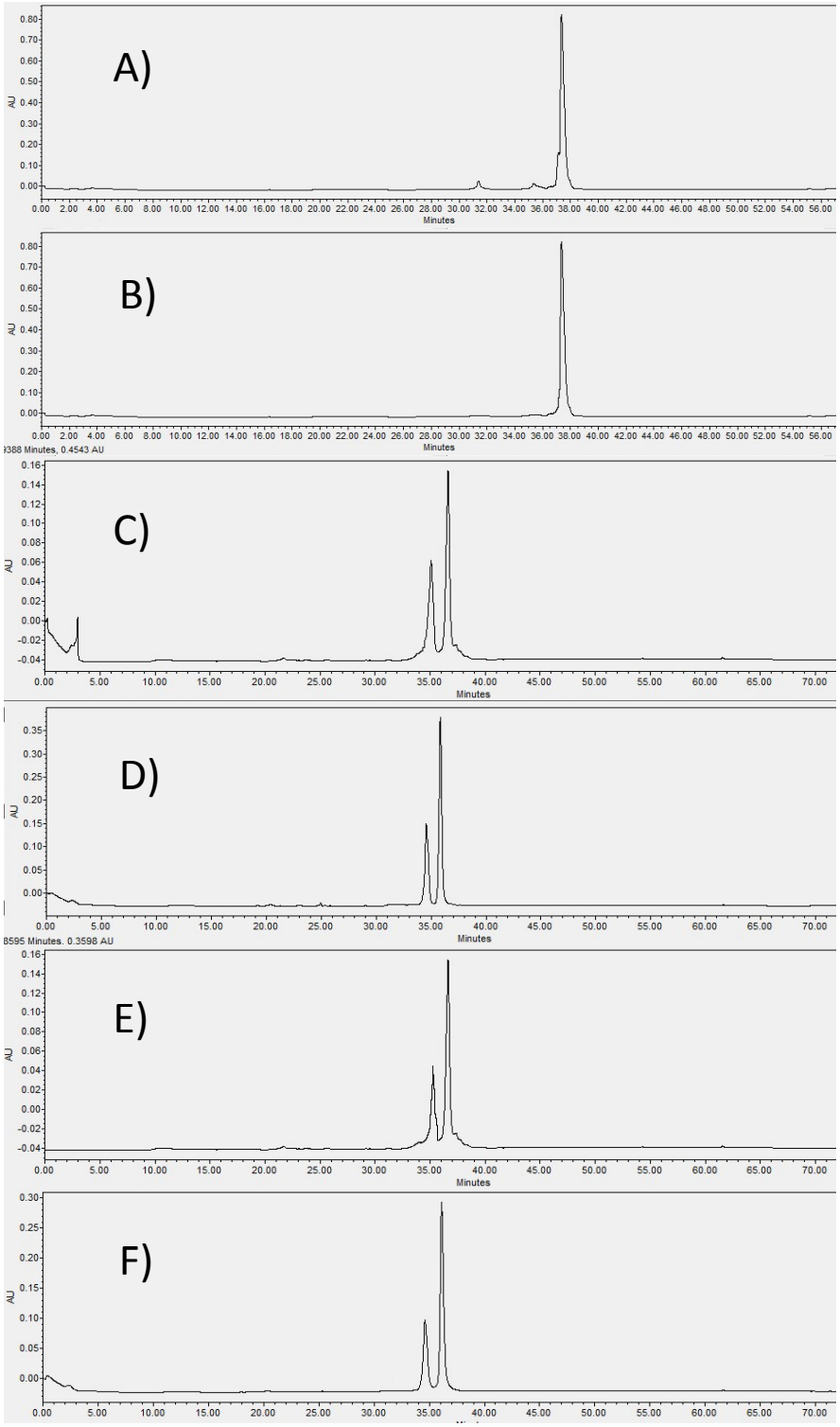

Figure S14 RP-HPLC trace of purified peptides with solvent gradient: A) F_6-G_8 with 99% purity from 5% ACN to 65% ACN, B) F_5Y-G_8 with 99% purity from 5% ACN to 65% CAN, C) F_4Y_2-G_8 with 99% purity from 5% ACN to 80% ACN, D) Y_2F_4-G_8 with 99% purity from 5% ACN to 80% ACN, E) F_3Y_3-G_8 with 99% purity from 5% ACN to 80% ACN, F) Y_3F_3-G_8 with 99% purity from 5% ACN to 80% ACN

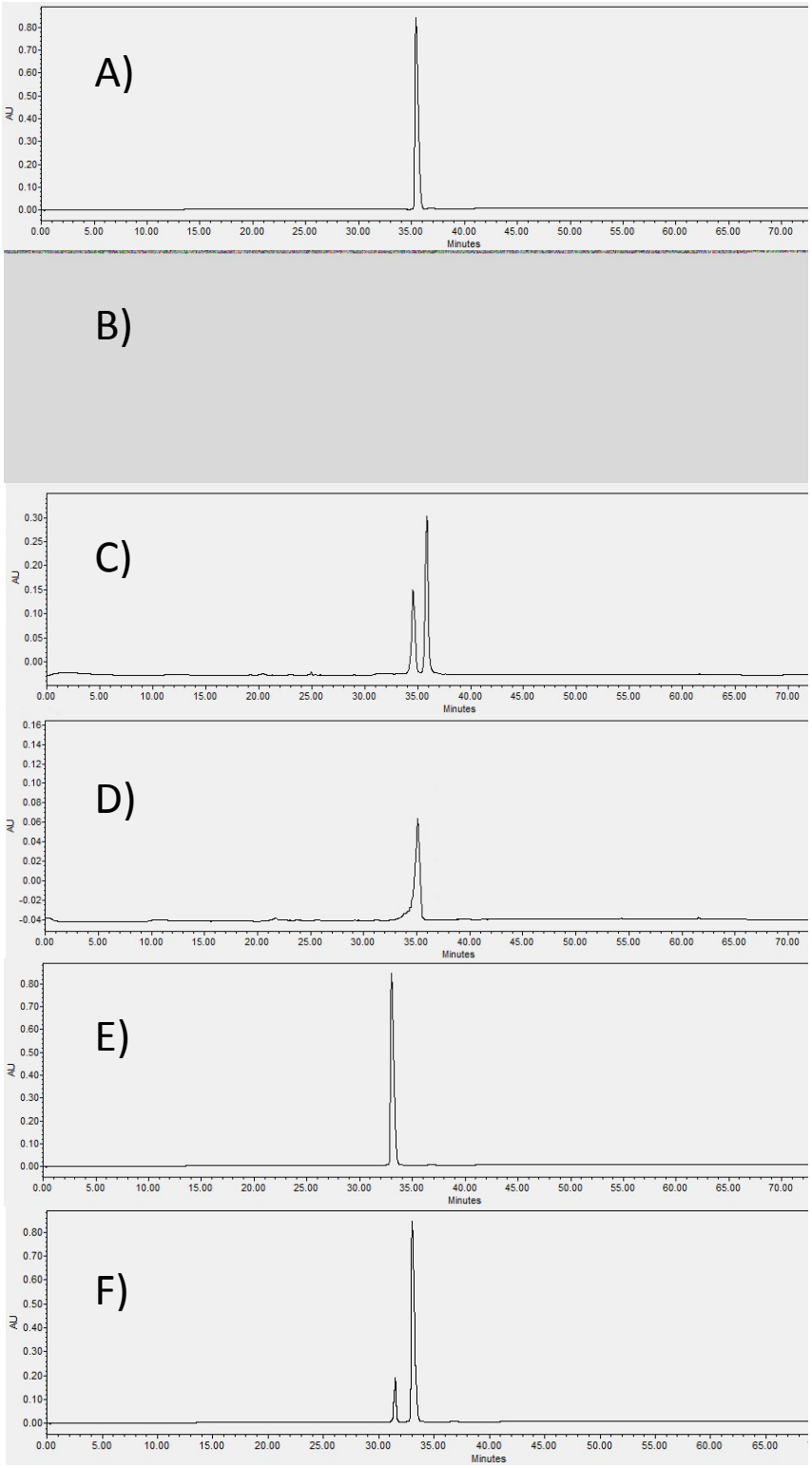

Figure S15 RP-HPLC trace of purified peptides with solvent gradient: A) F_5-G_8 with 99% purity from 5% ACN to 80% ACN, B) F_4Y-G_8 with 99% purity from 5% ACN to 80% CAN, C) F_3Y_2-G_8 with 99% purity from 5% ACN to 80% ACN, D) Y_2F_3-G_8 with 99% purity from 5% ACN to 80% ACN, E) F_2Y_3-G_8 with 99% purity from 5% ACN to 80% ACN, F) Y_3F_2-G_8 with 99% purity from 5% ACN to 75% ACN

Coarse-grained simulation details

In our coarse-grained model, the "H-bond" bead attraction strengths were chosen as the minimum interaction attraction strengths required to observe a shift in the transition point for F_4Y_2-$(POG)_8$ vs. F_6-$(POG)_8$. Therefore, the CG model captures the phenomenon of tyrosine substitutions effects on the LCST while also using a minimalistic approach. The relative H-bond bead attraction strengths involving Y and all other residues (X = V, P, F or G) were varied in order to obtain the minimum relative interaction strengths. Fig. S17 shows results for cases where A) all Y residues had H-bond bead attraction strengths that were 1.5 times the H-bond bead attraction strength of all other residues, B) all Y residues had H-bond bead attraction strengths that 1.75 times the H-bond bead attraction strength of all other residues, and C) H-bond bead attraction strengths that were 2.5 times the H-bond bead attraction strength of all other residues. A shift in the transition point was only observed for case C. Therefore, the optimized H-bond (i.e., LJ) parameters, ε^{HB}, were set at 50.4ε for Y-Y pairs, 31.9ε for Y-X pairs, and 20.2ε for X-X pairs where X can be any amino acid besides tyrosine, Y.

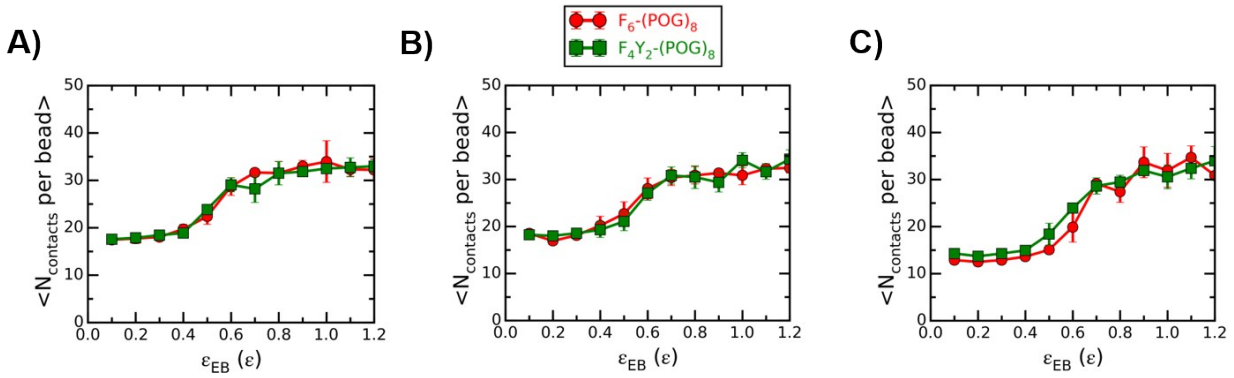

Figure S16: Ensemble average number of pairwise contacts per ELP coarse-grained (CG) bead vs. the strength of attractive pairwise interactions among ELP beads for (A) low H-bond bead attraction strengths ($\varepsilon_{Y\text{-}Y} = 1.5\ \varepsilon_{X\text{-}X}$), B) medium H-bond bead attraction strengths ($\varepsilon_{Y\text{-}Y} = 1.75\ \varepsilon_{X\text{-}X}$), and high H-bond bead attraction strengths ($\varepsilon_{Y\text{-}Y} = 2.5\ \varepsilon_{X\text{-}X}$).

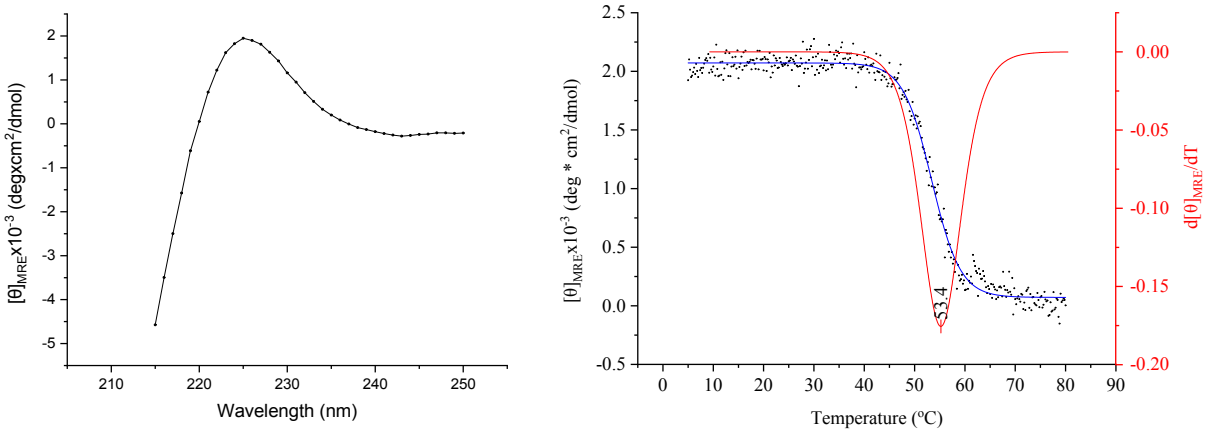

Figure S17 CD spectra showing a representative: Left: full-wavelength scan; Right: thermal unfolding profile at 225 nm for $(GPO)_8GG$.

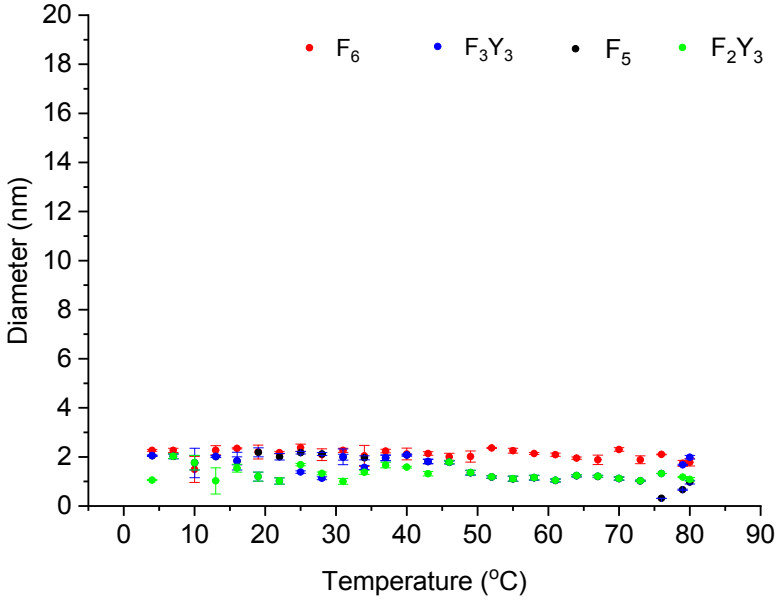

Figure S18 Average hydrodynamic diameter as a function of temperature obtained from dynamic light scattering (DLS) characterization for the represented ELP-CLPs. The error bars represent the standard deviation of three different measurements from a representative synthetic batch.

Table S1 Hydrodynamic diameter and the corresponding temperature for all the conjugates

ELP	CLP	Diameter (nm)	Temperature
F_6	$(GPO)_8GG$	~150 nm	31 °C
F_5Y		~120 nm	
F_4Y_2		~135 nm	
Y_2F_4		~145 nm	
F_3Y_3		~160 nm	
Y_3F_3		~175 nm	
F_5	$(GPO)_8GG$	~390 nm	40 °C
F_4Y		~400 nm	
F_3Y_2		~390 nm	
Y_2F_3		~390 nm	
F_2Y_3		~425 nm	
Y_3F_2		~430 nm	

Atomistic simulation details

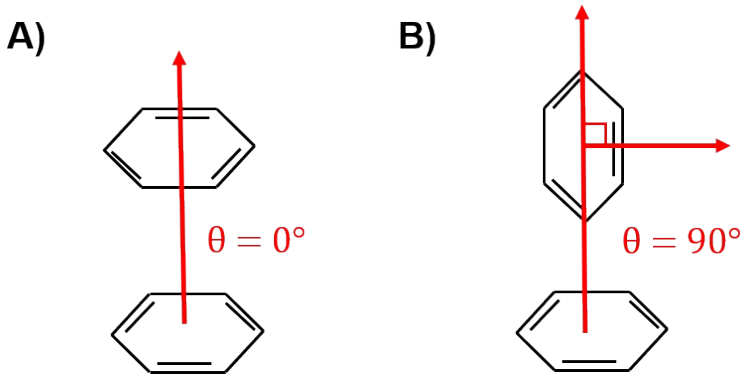

Figure S19: Schematic showing A) parallel stacking interactions between nearby aromatic rings and B) T- or Y-shaped (i.e. perpendicular) stacking interactions between nearby aromatic rings.

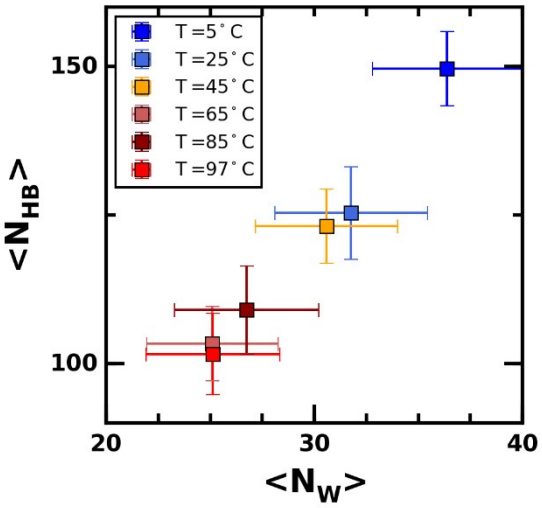

Figure S20: Hydration analysis of tethered F_4Y_2 showing the number of peptide-water hydrogen bonds ($<N_{HB}>$) plotted versus the number of water molecules in the 1st hydration shell of the peptide chain ($<N_W>$). Multiple hydration states are observed without an observable single LCST-like transition involving two distinct hydration states.

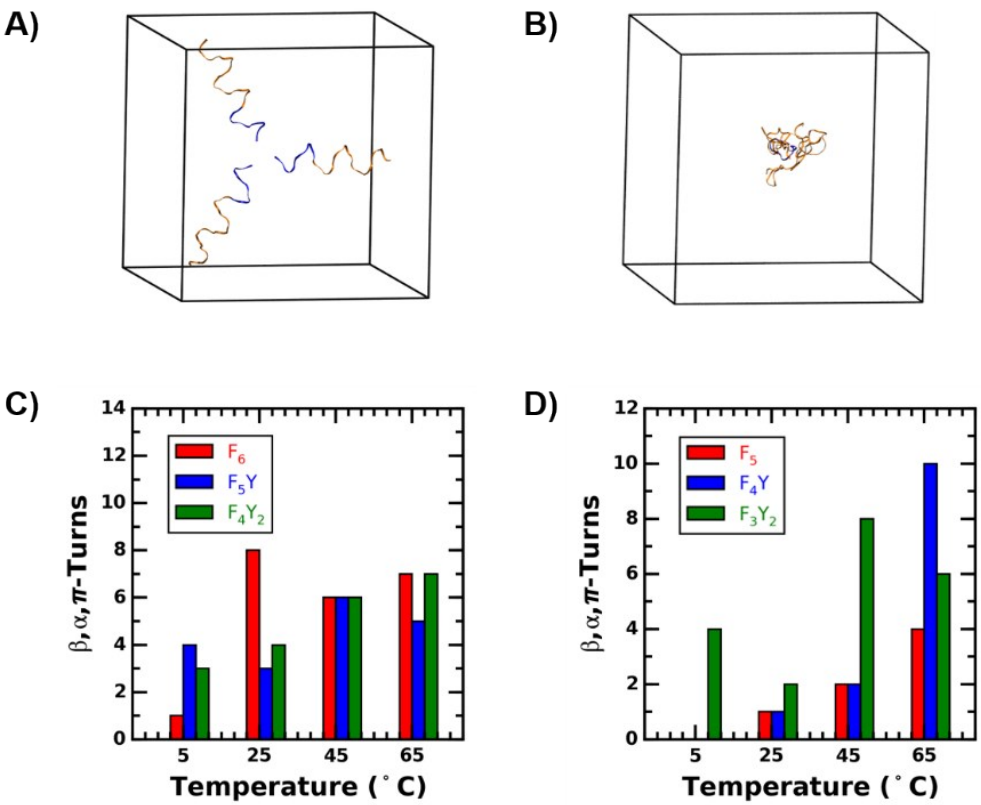

Figure S21: Simulation snapshots of tethered F_4Y_2 in the A) the initial β-spiral configuration and in the B) final configuration after 200 ns; this confirms that the initial configuration is not retained in the simulation. Plots of number of turn structures (β, α, and π) for C) tethered F_6, F_5Y, F_4Y_2, and D) tethered F_5, F_4Y, F_3Y_2 at the end of each simulation run (200 ns).

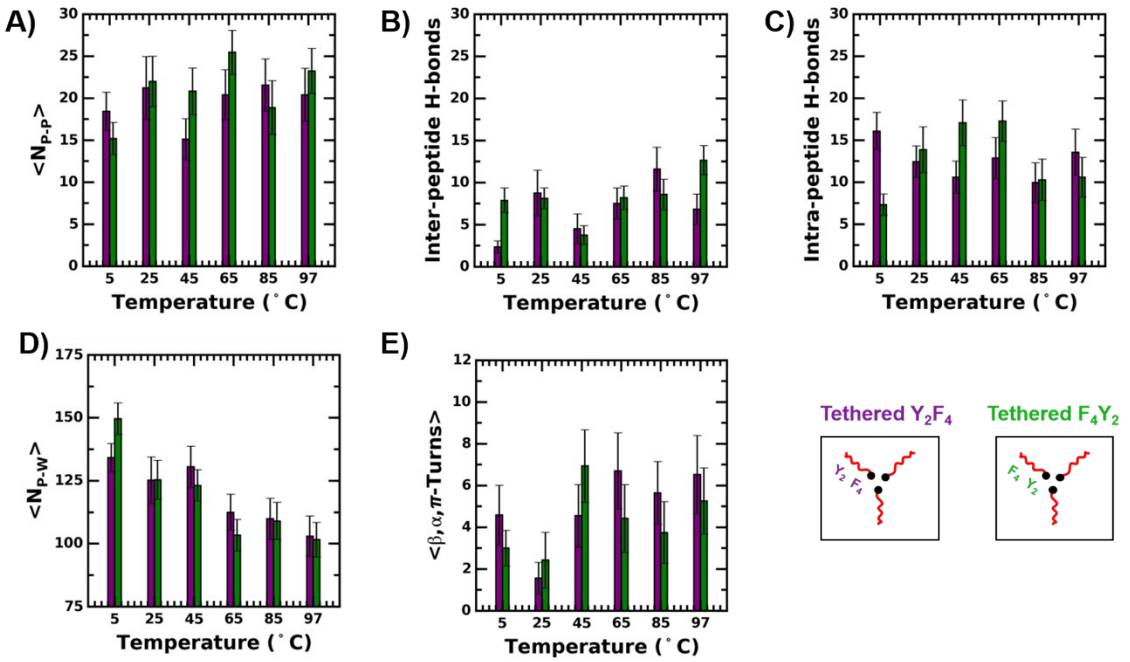

Figure S22: Hydrogen bonding analyses for tethered F_4Y_2, and Y_2F_4 (shown red, blue, and green, respectively) obtained from atomistic simulations: A) total peptide-peptide hydrogen bonds, B) inter-peptide hydrogen bonds, C) intra-peptide hydrogen bonds, D) peptide-water hydrogen bonds, and E) β, α, and π turns.

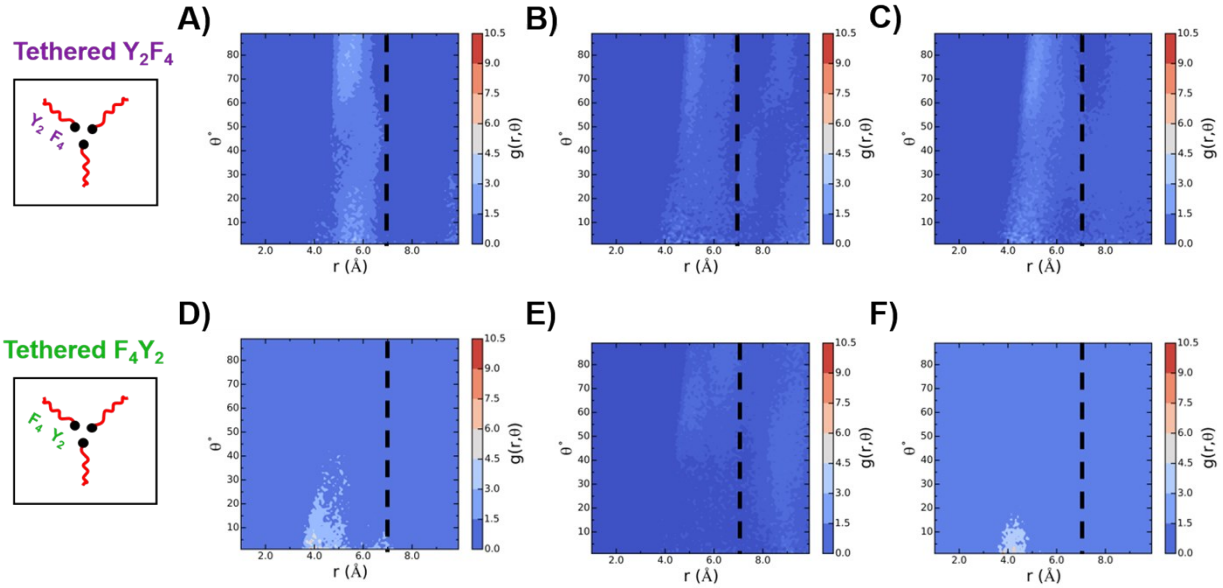

Figure S23: Effect of the tethering point/terminus on the π-π stacking of ELP 6-mers (F_6 series) at high temperatures: (A,D) 65 °C, (B,E) 85 °C, and (C,F) 97 °C.

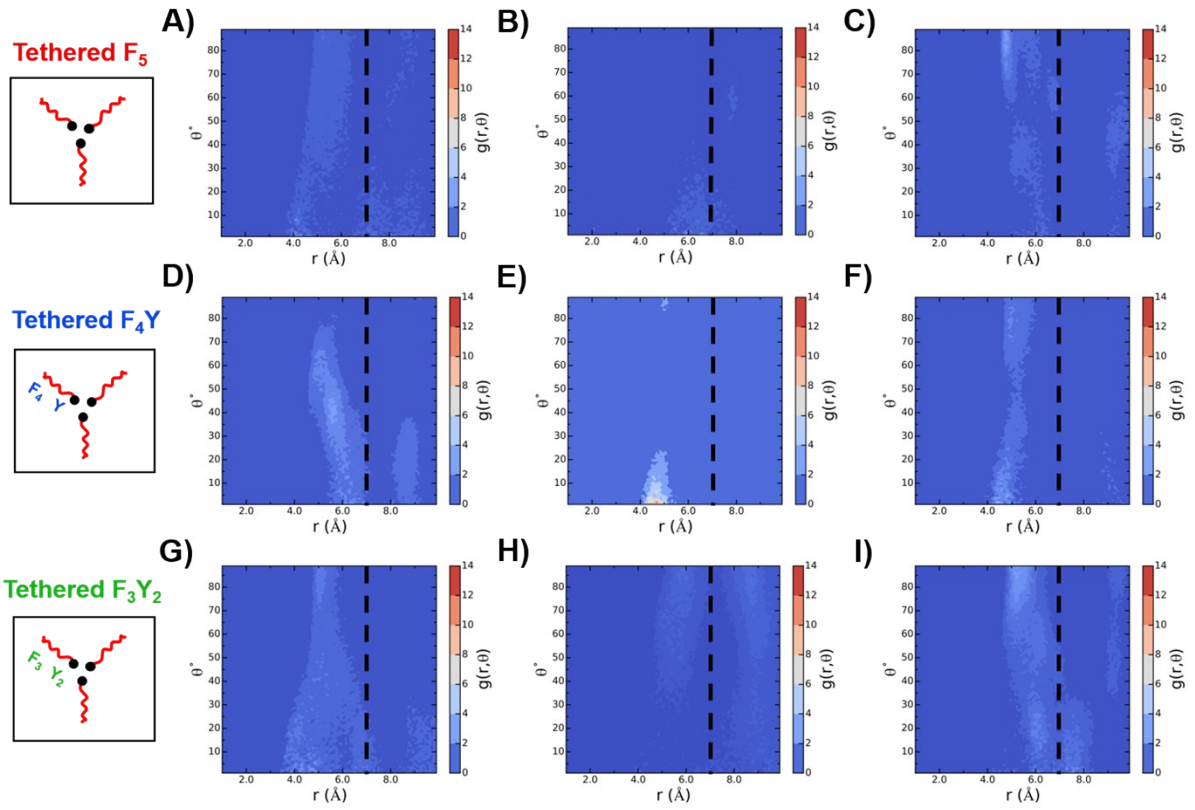

Figure S24: Effect of Y inclusion on the π-π stacking of ELP 5-mers at low temperatures: (A,D,G) 5 °C, (B,E,H) 25 °C, and (C,F,I) 45 °C.